JOURNAL OF APPLIED PHYSICS **115**, 144307 (2014)

# High quality single crystal Ge nano-membranes for opto-electronic integrated circuitry

V. A. Shah,[1,2,a)] S. D. Rhead,[2] J. E. Halpin,[2] O. Trushkevych,[2] E. Chávez-Ángel,[3,4] A. Shchepetov,[5] V. Kachkanov,[6] N. R. Wilson,[2] M. Myronov,[2] J. S. Reparaz,[3] R. S. Edwards,[2] M. R. Wagner,[3] F. Alzina,[3] I. P. Dolbnya,[6] D. H. Patchett,[2] P. S. Allred,[2] M. J. Prest,[2] P. M. Gammon,[1,2] M. Prunnila,[5] T. E. Whall,[2] E. H. C. Parker,[2] C. M. Sotomayor Torres,[4,7] and D. R. Leadley[2]

[1]*Department of Engineering, The University of Warwick, Coventry CV4 7AL, United Kingdom*
[2]*Department of Physics, The University of Warwick, Coventry CV4 7AL, United Kingdom*
[3]*ICN2-Institut Catala de Nanociencia i Nanotecnologia, Campus UAB, 08193 Bellaterra (Barcelona), Spain*
[4]*Department of Physics, UAB, 08193 Bellaterra (Barcelona), Spain*
[5]*VTT Technical Research Centre of Finland, P.O. Box 1000, FI-02044 VTT, Espoo, Finland*
[6]*Diamond Light Source, Harwell Science and Innovation Campus, Didcot, Oxfordshire OX11 0DE, United Kingdom*
[7]*Institució Catalana de Recerca i Estudis Avançats (ICREA), 08010 Barcelona, Spain*

(Received 23 January 2014; accepted 27 March 2014; published online 10 April 2014)

A thin, flat, and single crystal germanium membrane would be an ideal platform on which to mount sensors or integrate photonic and electronic devices, using standard silicon processing technology. We present a fabrication technique compatible with integrated-circuit wafer scale processing to produce membranes of thickness between 60 nm and 800 nm, with large areas of up to 3.5 mm$^2$. We show how the optical properties change with thickness, including appearance of Fabry-Pérot type interference in thin membranes. The membranes have low Q-factors, which allow the platforms to counteract distortion during agitation and movement. Finally, we report on the physical characteristics showing sub-nm roughness and a homogenous strain profile throughout the freestanding layer, making the single crystal Ge membrane an excellent platform for further epitaxial growth or deposition of materials. © *2014 AIP Publishing LLC*. [http://dx.doi.org/10.1063/1.4870807]

## I. INTRODUCTION

Integration of all manner of sensors, devices, and transducers onto a single chip is coined "system-on-a-chip"[1] and is a common aim in today's technology. However, this requires small scale structures to be fabricated using expensive processing techniques and materials. In this paper, we will outline a simple fabrication method for one of the basic micro-electro-mechanical systems (MEMS) components—the semiconductor membrane. These have been reported with thicknesses down tens of nanometers and typical areas in the order of 1 mm$^2$.[2]

This work is concerned with single-crystal germanium membranes formed on an initial silicon wafer. Single-crystal material has good thermal transport properties compared to poly crystalline and amorphous materials.[3] This is important for room-temperature MEMS devices, such as accelerometers, gyroscopes, and micromirror devices.[4] In the particular case of micromirrors, an essential component in a pico-projector system,[5] the surfaces need to be atomically smooth to increase the reflectance of visible light.[6] Flat MEMS surfaces are also required for other applications, such as integration of planar CMOS technology on membrane-type platforms.[7] The problem of membrane corrugation is thought to be due to the compressive strain direction within the layer. It could be overcome by using two identical layers of Ge with opposite strain directions, but here we show that a small amount of tensile strain is very effective in removing the corrugations.

As well as producing excellent membranes, the use of Ge-on-Si also allows the incorporation of III-V materials[8] on cheap Si substrates that could themselves be turned into membranes, in addition, there are other applications on membranes such as optoelectronic detectors,[9] optical modulators,[10] Ge lasers,[11] or even solar cells.[12] Germanium membranes of thickness 1.6 $\mu$m have previously been fabricated by Nam *et al.*[13] which were tensile strained to reduce the direct band gap for more efficient light emission. Devices for optoelectronic detection were fabricated on the membranes to demonstrate this effect, and later they demonstrated room-temperature electroluminescence opening the possibility for Ge lasers.[14] Audet *et al.*[15] demonstrated Fabry–Perot optical modulators on a Ge membrane operating at several GHz and Lagally *et al.*[16–19] investigated electro- and photoluminescence of Ge nano-membranes. Li *et al.*[34] also fabricated a Ge membrane in their initial work, but it was amorphous with corrugations.

Crystalline silicon membranes are currently fabricated using multiple expensive steps which may include: ion implantation, bonding, dry etching, or electrochemical etching.[7,20] Such membrane fabrication often starts from a silicon-on-insulator substrate which is then subjected to a combination of wet and dry etching.[21,22] However, membranes that survive the process often become warped and are corrugated due to strain within the topmost layers imparted by the buried oxide layer.[21] Other obstacles include membrane layer inter-diffusion and the

[a)]Email: vishal.shah@warwick.ac.uk.

 © 2014 AIP Publishing LLC

[This article is copyrighted as indicated in the article. Reuse of AIP content is subject to the terms at: http://scitation.aip.org/termsconditions. Downloaded to ] IP: 161.111.180.191 On: Tue, 15 Dec 2015 12:57:49

fragile nature of membranes in liquid etchants.[2] Simplifying the production techniques and making the whole process cheaper would clearly be of great interest. Our chosen technique is anisotropic wet etching, since wet etchants are cheaper and the process simpler than dry etching, a high Si etch rate is possible, and there is the added benefit of the anisotropy which allows crystal planes to be used for etch definition.

In this paper, we outline a simple method of fabricating single-crystal Ge membranes by wet etching and a second method that combines wet and dry etching in a scalable, IC compatible process. We characterize the quality of these Ge membranes by a range of techniques and confirm their appropriateness as platforms. As an example, Figure 1(a) shows a compressively strained Ge[23] layer grown epitaxially on Si via a strain tuning buffer[24,25] with the aim of improving hole mobility, however, the large dislocation density in the top-most strained layer means that leakage by dislocation conduction could be an issue.[26–28] We showed previously[29] that electrical isolation in such a Ge-on-Si structure can be improved by suspending the Ge layer, interpreting this as being due to removing the conduction path through the network of misfit dislocations (Figure 1(b)). In this report, we present further evidence that these misfits are indeed removed. The quality of these strained epitaxial layers can therefore be improved through suspension, enhancing their potential for device applications.[29,30] The planarity of the single-crystal membranes makes them amenable to current processing technologies and the opportunity for subsequent over-growth of further epitaxial layers allows the advantages of epitaxial heterostructures and of fabricating devices on membranes to be combined.

## II. MEMBRANE FABRICATION AND INITIAL CHARACTERIZATION

### A. Background

Si membranes[31] have most commonly been fabricated by etching through a mask layer on the back-side of a Si (001) wafer by a wet anisotropic etchant, such as potassium hydroxide (KOH), tetramethylammonium hydroxide (TMAH), or ethylenediamine pyrocatechol (EDP)[32] towards the top-side of the wafer where an etch stop layer is defined to protect the membrane layer above. Etch masks or etch-stop layers[33] are frequently made from insulating layers such as $SiO_2$ or $Si_3N_4$ and/or highly doped semiconductors where the etch rate significantly drops with increasing dopant concentration.[33] Both the etch stop and masking layers can be the same material, but creating these mask layers requires high temperatures (>600 °C) either to ensure incorporation of a high level of dopant or to grow a good quality dielectric layer that completely resists the etchant. However, if such processes were applied with heterostructures on a membrane, the thermal treatment would result in inter-diffusion of the heterostructure, membrane material, and substrate, hence ruining the layer definition. Consequently, development of a lower temperature mask process is attractive.

Li *et al.*[34] used amorphous and polycrystalline Ge layers as mask layers due to the etching selectivity of KOH and TMAH of Si over Ge. They previously reported that polycrystalline Ge has a low etch rate of approximately 0.09 nm $min^{-1}$ within a 42% KOH etchant at 62 °C, whereas it is well known[33] that Si has a relatively high etch rate of approximately 300 nm $min^{-1}$ for similar conditions. Pure Ge can be deposited epitaxially, using either molecular beam epitaxy or chemical vapor deposition (CVD) at temperatures as low as 250 °C where the layer quality is good enough to fully resist alkaline anisotropic etchants, thus solving the problem of low temperature masking. Consequently, if a low temperature tensile strained crystalline Ge layer could be fabricated (with the tensile strain eliminating the corrugations[35]) it could be the ideal membrane material.

In a previous study,[36] we investigated the two-temperature Ge growth method for producing a high-quality crystalline layer on Si(001). Ge has a lattice parameter 4.2% larger than Si and in low temperature epitaxial growth, the first few monolayers of Ge conform to the Si substrate lattice parameter, which compressively strains the Ge. As the thickness of the layer is increased, dislocations form to relieve the strain. A subsequent higher temperature layer enhances this effect until the Ge is 100% relaxed during growth, and is

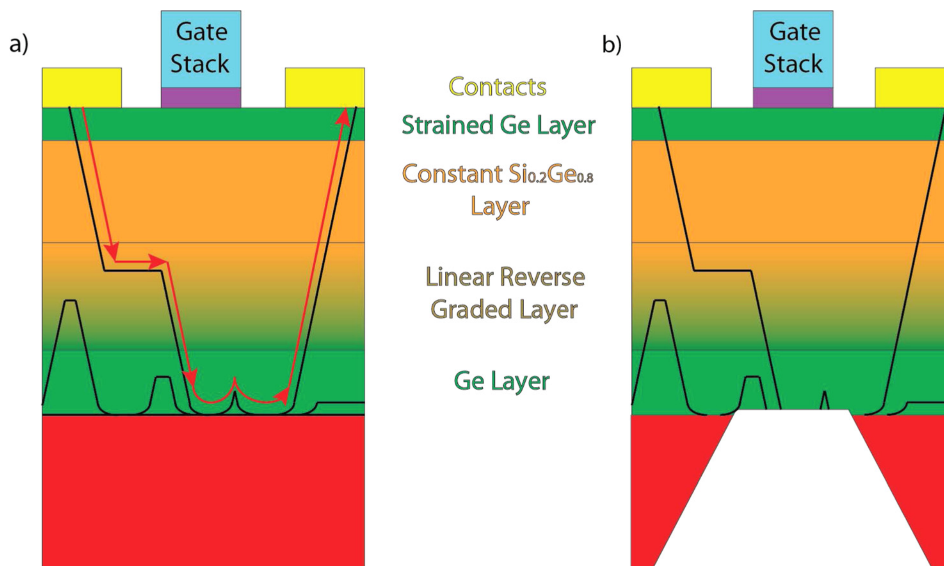


FIG. 1. Shows the possible application of the membranes to incorporate heteroepitaxial layers into their design, this example shows a MOSFET device using a strained Ge layer on a reverse graded buffer. (a) shows the heterostructure and the possible leakage paths along the dislocations (red), (b) removes these dislocation paths by placing the device onto a membrane.

[This article is copyrighted as indicated in the article. Reuse of AIP content is subject to the terms at: http://scitation.aip.org/termsconditions. Downloaded to ] IP: 161.111.180.191 On: Tue, 15 Dec 2015 12:57:49

hence strain neutral at this point. However, when cooling from the high growth temperature (>650 °C) the dislocations become immobile, and since Ge has a larger thermal expansion coefficient than Si, the Ge lattice parameter will not contract as much as the Si substrate, thereby imparting tensile strain into the Ge layer. From this work, we found conditions to separately create a compressive and tensile strained Ge layer of equal thickness on a Si (001) substrate for membrane fabrication.

### B. Epitaxial layer growth

This investigation starts with 4 in. diameter silicon (001) wafers. These wafers were polished on both sides so that structures could be created with a compressive (c-Ge) layer grown on one surface and a tensile (t-Ge) layer on the other surface. The Si wafers were low resistivity (10–25 Ω cm) and 300 $\mu$m thick. The germanium layers were grown epitaxially, by reduced pressure CVD (RP-CVD) in an ASM Epsilon 2000E system using germane as a precursor.[37] Prior to growth of Ge, the native oxide of the wafer was desorbed at 1000 °C for 2 min. Initially, the t-Ge layer was grown on the front-side of the wafer. We used the two-temperature method: a 100 nm thick Ge layer was first deposited at 400 °C, followed by a 600 nm layer at 670 °C, with a final anneal at 830 °C for 10 min. As the t-Ge growth included a higher temperature process than the c-Ge growth, it had to be performed first to avoid affecting the latter. In order to grow the c-Ge layer on the back-side, the wafer was then cooled to room temperature, unloaded to a nitrogen atmosphere (within a Class 10 clean area), turned over and reloaded into the growth chamber for a 700 nm deposition at 400 °C. The wafer turning process was carried out as quickly as possible to ensure the surface remained $H_2$ terminated and no native oxide was formed. A second high temperature $SiO_2$ desorption anneal was therefore not needed before the back-side growth, which could otherwise have compromised the earlier front-side growth. A schematic diagram of the structure is shown in Figure 2, together with cross-sectional transmission electron microscopy (XTEM) images of the top-side and back-side Ge layers that were obtained using a JEOL 2000FX TEM at 200 kV in the (000) diffraction condition. From these images, we determined that both Ge layers are 700 nm thick and fully crystalline, although the c-Ge layer has a significantly higher number of dislocations.

The relaxation and composition of the layers was determined by X-ray diffraction (XRD) using a Philips X'pert MRD Pro single crystal high resolution X-ray diffractometer. Reciprocal space maps (RSM) were performed along the symmetrical (004) and asymmetrical (224) orientations, which allowed the in- and out-of-plane lattice parameters to be calculated. The c-Ge layer was measured to have a strain of $-0.121 \pm 0.042\%$, i.e., with a slight compressive strain. The t-Ge layer had a measured relaxation of $0.175 \pm 0.042\%$, therefore being slightly tensile strained. We have investigated both layers as possible membranes.

### C. Simple wet etching process

A *compressively strained Ge membrane*, using the layer grown on the back-side of the wafer, was first prepared by using the HT t-Ge layer as an etch mask to selectively remove the Si substrate (Figure 3(a)). A 1 mm square window was made in the t-Ge by masking with chemically resistive Apeizon W (black wax) and then etching with $HF:H_2O_2:CH_3COOH$ in a 1:2:3 ratio for 30 s at $19 \pm 1$ °C. This etches Ge at a rate of 4 $\mu$m min$^{-1}$ but only etches Si at $\sim$1 nm min$^{-1}$, so essentially stops at the Si surface.[38] After a de-ionised water (DI) rinse, the Apeizon W is removed in a toluene solvent bath with sonic agitation; the surface is cleaned by another clean toluene dip, followed by an acetone rinse and finally dried by passing $N_2$ over the surface. The Si under this window is then removed by a deep anisotropic etching process using 30% KOH at $100 \pm 2$ °C for 100 min. This selectively etches Si at a rate of 3.7 $\mu$m min$^{-1}$ while only attacking fully crystalline Ge at about 4 nm min$^{-1}$.[33]

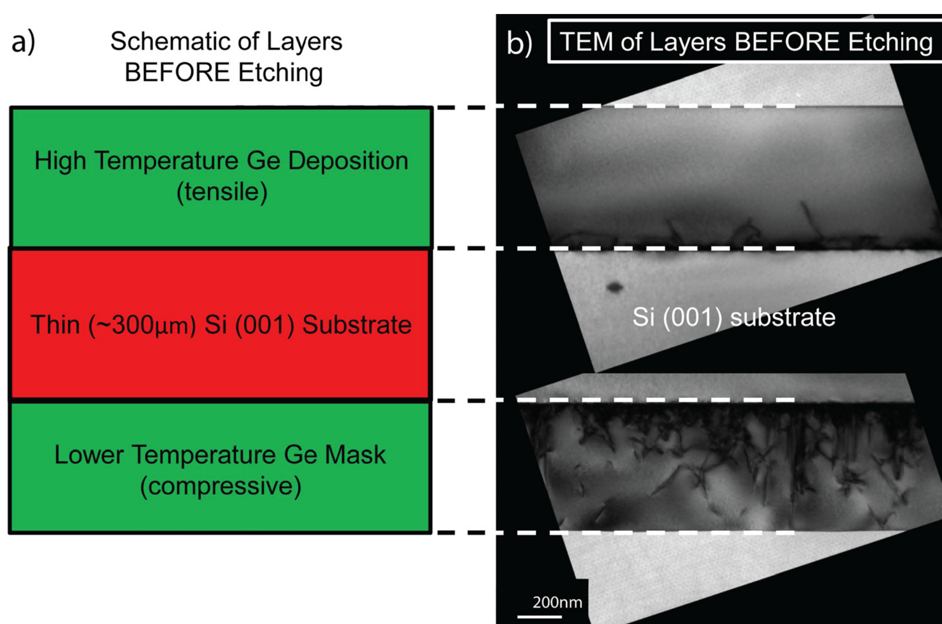


FIG. 2. (a) Schematic diagram of the layer scheme and (b) XTEM of the top-side and back-side Ge layers.

[This article is copyrighted as indicated in the article. Reuse of AIP content is subject to the terms at: http://scitation.aip.org/termsconditions. Downloaded to ] IP: 161.111.180.191 On: Tue, 15 Dec 2015 12:57:49

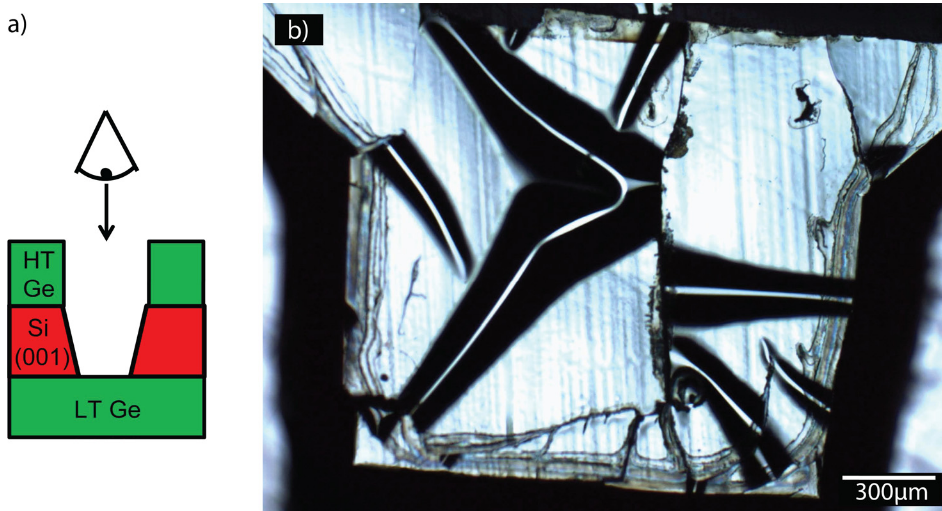


FIG. 3. (a) Schematic and viewing angle of etching profile for the LT Ge membrane with nominal thickness of 700 nm and (b) DIC Nomarski imaging of the etched surface of the compressive LT Ge layer.

Finally, heated DI water is flowed over the surface to neutralize the reaction.

Figure 3(b) shows optical images of the etched surface of the low-temperature (LT) c-Ge membrane, viewed with a Zeiss Axio optical microscope in both normal optical and differential interference contrast (DIC) modes. The etched area is close to 1 $mm^2$ and three main features can be observed on an otherwise smooth surface: short range ripples, large scale ripples, and cracking. The small scale ripples cannot be seen in the normal optical images, which suggests their height is in the 10 nm–100 nm range. By contrast, the main large ripple has a height of $\sim 5\,\mu$m, which we determined by varying the focal length of the microscope. The cracking seen in this image shows that the membrane is quite fragile, which precludes further examination by scanning electron microscopy (SEM).

A *tensile strained Ge membrane* was next prepared using the layer grown on the front-side of the wafer. This time the LT c-Ge layer was used as the etch mask in a similar process to that described above (Figure 4(a)). In an optical image (Figure 4(b)) no long range ripples are seen, and in a corresponding DIC image (Figure 4(c)) no short range ripples are observed. Finally, no cracks are observed in this membrane, leading it to being supported on all sides. Handling of this membrane suggests that it is quite robust.

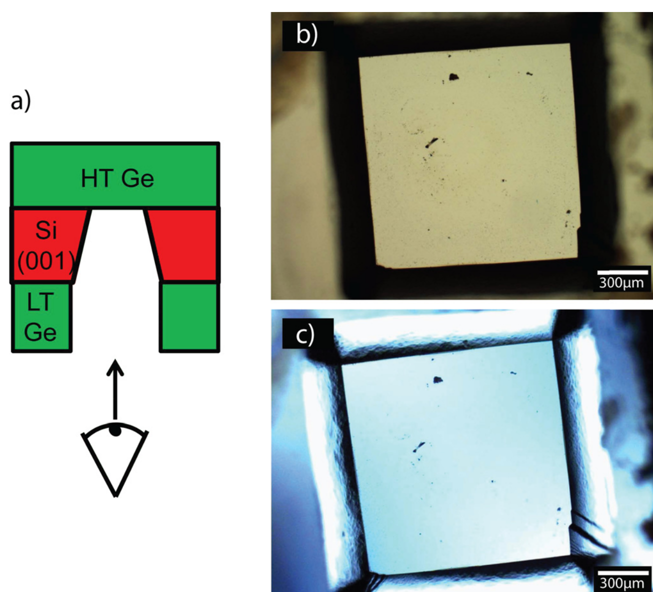


FIG. 4. (a) Schematic and viewing angle of etching profile for the HT Ge membrane, (b) Optical imaging of the etched surface of the compressive LT Ge layer, and (c) DIC Nomarski image of the same sample.

The surface quality and thickness of the t-Ge membrane formed has been examined by deliberately bursting it and viewing in a ZEISS SUPRA55VP FEGSEM, with an acceleration voltage of 15 kV. Figure 5(a) shows these remnants attached to an SEM stub with the etched side face up; the overall outline of the membrane is highlighted. The higher magnification image of Figure 5(b) shows the side profile of a membrane slice, from which the etched surface of the membrane can be seen to be generally smooth and the membrane thickness can be estimated to be 600–700 nm, although the sample tilt limits the accuracy of this measurement. A few etch islands of sub-micron lateral dimension can be seen in Figure 5(b). This is typical of the rest of the surface, but their height is tiny compared to the dimensions of the membrane and so these islands can be dismissed as insignificant.

### D. Scalable two-step dry/wet etching process

Although this simple wet-etching fabrication technique produces a high quality membrane, it could not be easily scaled up for mass production; it also leaves potassium alkali metal ions on the etch surface. We have therefore developed an alternative process using TMAH, which is an IC compatible anisotropic etch. Etch rates with TMAH are, however, generally slower than with KOH,[39] so deep reactive ion etching (DRIE) has been employed to remove most of the Si, leaving just the final $50 \pm 25\,\mu$m of Si below the Ge layer to be removed by wet etching in TMAH.

Epitaxial growth of the second batch was identical to the first, and this time included wafers with both nominally 700 nm and 200 nm thick t-Ge layers to produce thinner membranes.[36] As previously, a 400 nm thick c-Ge layer was grown on the back-side of each wafer at lower temperature. On this, an $Al_2O_3$ layer was deposited by atomic layer deposition, using

[This article is copyrighted as indicated in the article. Reuse of AIP content is subject to the terms at: http://scitation.aip.org/termsconditions. Downloaded to ] IP: 161.111.180.191 On: Tue, 15 Dec 2015 12:57:49

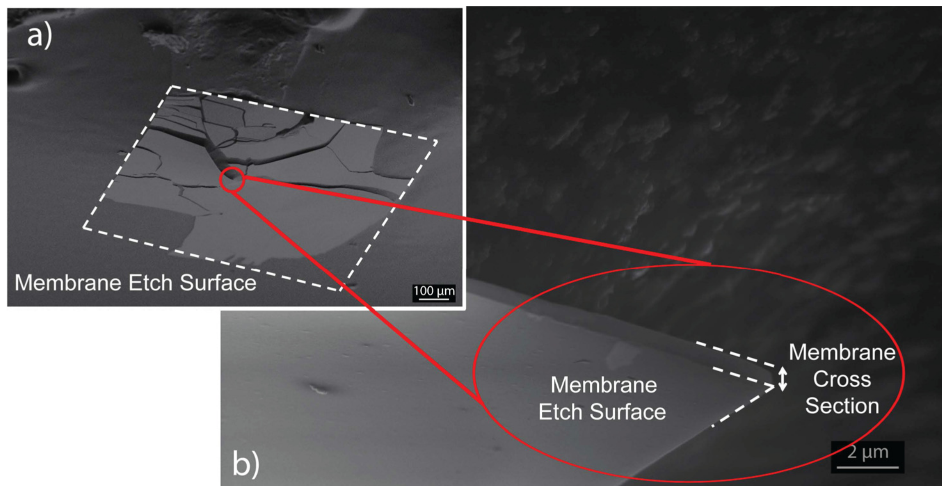


FIG. 5. (a) Low magnification of the etched HT Ge membrane surface (tilted) once intentionally broken to examine cross sectional thickness and (b) Higher magnification imaging of the etched surface where the full thickness of the tensile HT Ge layer can be seen.

a Picosun SUNALE(TM) R-150B with trimethylaluminum and $H_2O$, to serve as an etch mask for the LT Ge. It was patterned using AZ5214E photoresist and a Karl Suss MA6 mask aligner and developed in AZ726 MiF and then etched using a buffered hydrofluoric acid etch at 30 °C. The LT Ge was then selectively wet etched to the Si surface of the wafer back-side with the same $HF:H_2O_2:CH_3COOH$ etch, exposing windows ready for deep Si etching. After stripping the remaining resist, the wafer was placed inside an surface technology systems Silicon ICP etcher with a Bosch[40] process alternating between a $SF_6$ and $O_2$ mix, and $C_4F_8$ gas at 15 W to remove approximately $275 \pm 25\,\mu$m of silicon. The etch depth which was confirmed by changing the focal height of an optical microscope. The final step in membrane fabrication was to place the whole patterned wafer into an 80 °C 25% TMAH heated bath, which has been reported to have a Si etch rate of $0.45 \pm 0.02\,\mu$m $\text{min}^{-1}$.[39] To ensure that the Si was completely removed from the back-side of the Ge layer, and in some cases to thin the Ge membrane itself, the wafer was etched for up to 420 min. From interferometry measurements using a Reflectometer Sci-soft Filmtek 2000M (with wavelengths 380–890 nm), the etch rate of Ge in the TMAH bath was measured to be $0.18 \pm 0.09$ nm $\text{min}^{-1}$, which is much lower than the 40 nm $\text{min}^{-1}$ reported by Li for polycrystalline Ge. Utilizing this low etch rate, we perform a controlled thinning of the nominal 200 nm Ge layer to create thin (measured to be ~250 nm) and ultra-thin (~64 nm) Ge membranes in addition to the thick (measured to be ~800 nm) membranes. The method of determining actual membrane thickness is described in Sec. III.

A plan-view SEM image of the ultra-thin membrane is shown in Figure 6(a). Electron transparency through the ultra-thin membrane produces a contrast between the suspended membrane and the bulk frame, which reveals the large lateral area of 3.5 $\text{mm}^2$. Figure 6(b) shows an SEM image of the ultra-thin membrane when burst from the surrounding frame, from which an approximate thickness of 56 nm can be measured, although this is not accurate due to tilt of the layer. White light interferometry measurements place the thickness of this membrane as $64 \pm 2$ nm, reduced from the initial thickness of 250 nm due to controlled thinning.

The fabrication of these membranes was on a wafer scale and approximately 50% of the thin and ultra-thin membranes survived the processing. For the thicker 800 nm layer, the yield was approximately 80%.

## III. MEMBRANE OPTICAL PROPERTIES

As a prelude to the vibrational measurements that use laser excitation, described in Sec. IV, it was necessary to measure the power absorption ($A$), reflection (R), and transmission (T) coefficients in the spectral range between 450 nm and 1000 nm. Excitation was via a tungsten-halogen lamp (Ocean Optics HL-2000), with a spot size of about 100 $\mu$m, and detection used a high-resolution HORIBA Jobin-Yvon spectrometer equipped with a charge-coupled device having a spectral resolution better than 0.1 nm. The power absorption of the membranes was computed according to: $A = 1 - R - T = 1 - P_R/P_I - P_T/P_I$, where $P_R$ is the

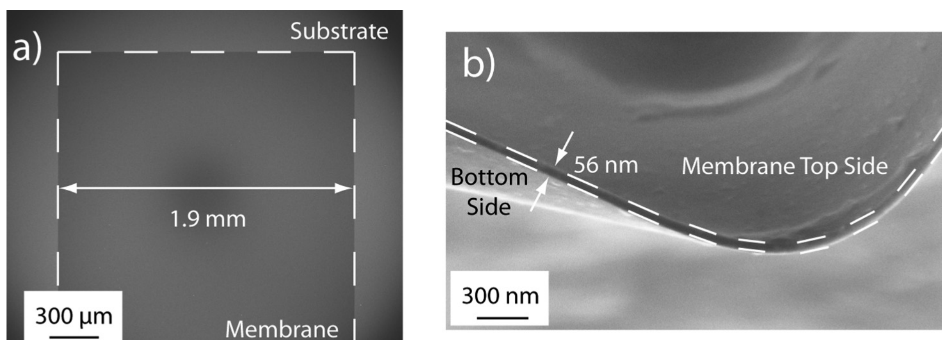


FIG. 6. The 64 nm membrane: (a) plan view SEM showing the large area of the membrane where electron transparency allows contrast between the membrane and its bulk frame. (b) A side view of a burst 64 nm membrane to show the dimensions of the cross section, showing a tilted thickness of 56 nm.

[This article is copyrighted as indicated in the article. Reuse of AIP content is subject to the terms at: http://scitation.aip.org/termsconditions. Downloaded to ] IP: 161.111.180.191 On: Tue, 15 Dec 2015 12:57:49

reflected power, $P_T$ is the transmitted power, and $P_I$ is the incident power on each membrane. All measurements were performed at 294 K.

Figure 7 shows $R$, $T$, and $A$ for the thick and thin Ge membranes as a function of wavelength. In the spectral region $\lambda < 600$ nm, both the thin and thick membranes have the same $A$, $R$, and $T$, which arises from the small penetration depth of Ge in this spectral region[41] ($1/\alpha \approx 50$ nm), i.e., the incident photons mostly probe the surface of the membranes. As the wavelength increases so does the penetration depth and both top and bottom surfaces of the membrane start playing a role, this leads to the transmission threshold changing from 675 nm in the thick membrane to 600 nm in the thin. Reflection of the incident beam at both surfaces leads to interference effects, as in an optical Fabry-Pérot cavity. The membrane thickness $d$ can be obtained from the condition of minimum reflected intensity in such a cavity, $2nd = m\lambda_m$ (integer $m$ gives reflection minima, not maxima, because of a $\pi$ phase change on internal reflection), provided that the strong frequency dependence of $n$, the refractive index in Ge, is included. This yields thickness values of 798 nm and $248 \pm 50$ nm for the membranes of nominal 700 nm and 200 nm thickness.

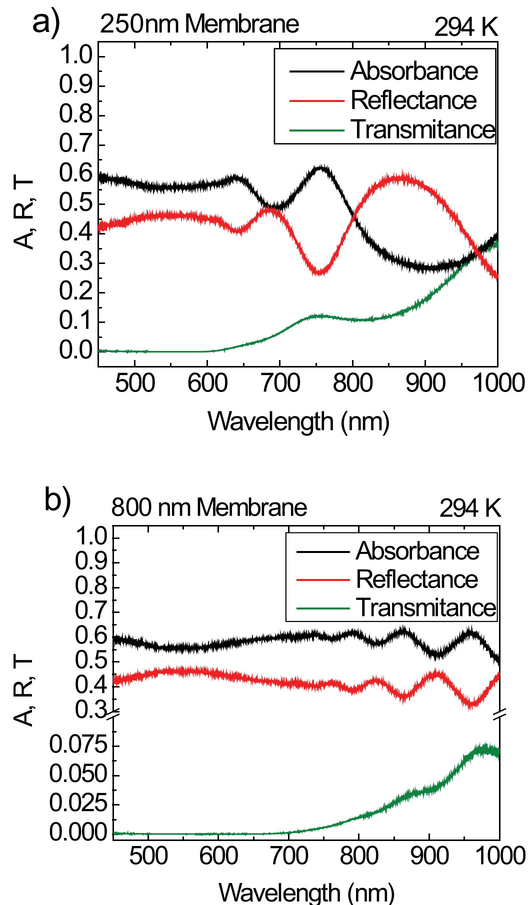


FIG. 7. Absorption (A), Reflection (R), and Transmission (T) coefficients for two Ge membranes with (a) 250 nm and (b) 800 nm in thickness at 294 K. The oscillations for larger wavelengths arise from interference effects in the membranes.

## IV. MEMBRANE VIBRATIONAL PROPERTIES

The quality factor of MEMS devices is an important consideration when deciding on the optimal membrane material. Among current MEMS devices, stressed silicon nitride membranes have the highest reported mechanical quality factors to date, with Q-factors of up to $10^6$.[42–46] However, silicon nitride is not electrically conductive, so these are not suitable for applications where an electrical readout is required. Recently, carbon structures have attracted interest as suitable materials for MEMS. Carbon allotropes have extremely high Young's moduli, are particularly light and thin (graphene being just one atom thick sheet) and therefore generated a lot of interest as materials for nanoelectromechanical systems (NEMS). Single and double walled carbon nanotube (CNT) resonators have Q factors of 40–200,[47] while multi-walled CNTs and CNT fibers reported Q factors reach 250–2500.[48–51] Graphene resonators exhibit slightly higher Q factors from several hundred[52–54] to over a thousand,[55,56] while graphene oxide has even higher Q factor of 4000.[57] Recently, Q factors as high as $10^5$ were demonstrated for graphene membranes.[58] Si is often used in MEMS, with the reported Q-factors for silicon resonators of the order of $1.4–1.6 \times 10^5$.[59,60] Silicon in combination with germanium, and germanium on its own, have also been used in a polycrystalline form, with $Si_{0.35}Ge_{0.65}$ MEMS having Q = 70 in air and 14 000 in vacuum, and poly Ge having Q = 45 in air and 30 000 in vacuum at room temperature.[61] Q-factors vary greatly when measured in atmosphere or in a vacuum. The air induces viscous damping on the resonators, and the effect is larger for large area resonators; at ambient pressure smaller membranes have higher Q-factors than larger membranes due to this damping.[62] This explains the difference in the Q-factor for poly Ge MEMS devices given above.[61] Although large Q factors are required for resonators, for a stable platform, a low Q-factor is required. A low Q-factor will help isolate the devices placed on the platform from external noise and vibrations, so that their electrical/optical/mechanical properties remain stable.

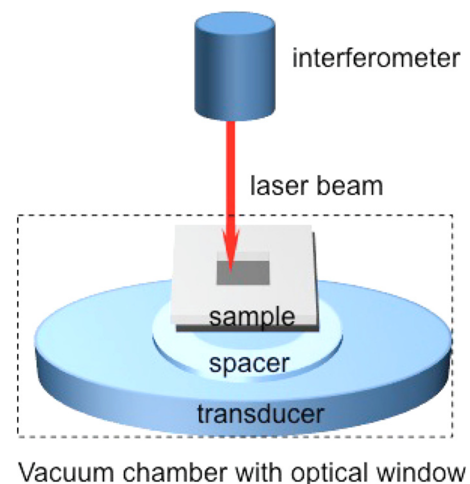


FIG. 8. Experimental arrangement: The sample membrane is attached to the transducer and the resulting vibrations of the membrane are studied using the laser interferometer. The vacuum chamber is used to control pressure.

[This article is copyrighted as indicated in the article. Reuse of AIP content is subject to the terms at: http://scitation.aip.org/termsconditions. Downloaded to ] IP: 161.111.180.191 On: Tue, 15 Dec 2015 12:57:49

The vibrational properties of our 800 nm thick membrane were studied using laser interferometry techniques, with the setup shown in Figure 8. Vibrations in the membrane were excited by mounting it on a broadband (PZT) piezoelectric transducer (from Physik Instrumente), with a central frequency of 2 MHz, that was coupled to the substrate and driven over a range of frequencies by a function generator. The vibration of the substrate induced vibration in the membrane, the displacement of which was monitored using an Intelligent Optical Systems, Inc. (IOS) AIR-1550-TWM two wave mixer interferometer, with a bandwidth of 125 MHz. The measurement system was calibrated and gives the absolute out-of-plane displacement of the membrane after vibration. The membrane and transducer were placed in a vacuum chamber with an optical window, transparent to the wavelength of the laser interferometer. The pressure in the chamber was varied from atmospheric down to $5 \times 10^{-4}$ millibars at which point damping though atmospheric gases becomes negligible.[62] A low power (100 mW), long wavelength (1550 nm) laser was used to accurately measure the vibration and minimize energy absorption that would occur with shorter wavelengths due to the small bandgap of 0.67 eV in Ge.

The vibrational spectra of the 800 nm membrane are presented in Figure 9 for ambient pressure and in vacuum; note that resonances present at the substrate are due to resonances in the transducer. At low pressure, the resonant peaks become more pronounced, as expected. Damping in air is expected to shift the resonant peaks to a lower frequency, by about 16% compared to measurements in vacuum.[63] However, only a very small frequency difference is observed between our measurements at low and high pressures. This is probably because the resonant peaks in the low pressure measurements were also shifted to lower frequencies, by sample heating from optical absorption that could not be dissipated due to the limited thermal exchange at low gas pressures. 3.2% of the incident power is absorbed by 800 nm layer of Ge, and at atmospheric pressure, this leads to a temperature rise of less than 1 K. However, at low pressures the heating becomes more significant due to reduced convection cooling. Heating manifests itself in the lowering of vibrational frequencies due to reduction of the tensile strain in the membrane arising from the mismatch of expansion coefficients of the Si substrate and the Ge layer. This could also slightly reduce the experimentally measured Q factors of the membrane.

The first vibrational mode and its Q-factor are shown in Figure 10 for measurements at (a) atmospheric pressure and (b) in vacuum. It can be seen that the Q-factor increases significantly as the pressure is reduced from approximately 50 at atmospheric pressure to over 3000 at $5 \times 10^{-4}$ millibars. The value at low pressure is an underestimation of the true value, due to the influence of sample heating. The measured Q-factors are lower than the reported membrane behavior for poly Ge and Si in vacuum, but have similar Q values at atmospheric pressure.[61,64] This is because at atmospheric pressure, the limit on Q factor values is determined by damping due to the air, while in vacuum damping is governed by different mechanisms such as clamping losses, thermoelastic and phonon-phonon interactions, as well as losses at the internal defects in the films. In the case of the studied membrane which has relatively low Q factors, high crystalline quality, and low tensile stress (good matching between the

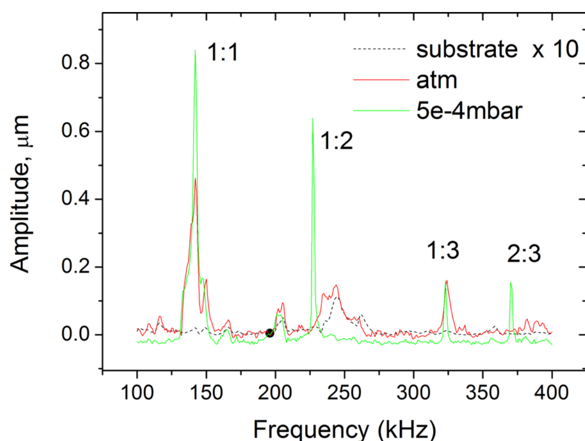


FIG. 9. Vibrational spectra of the 800 nm membrane showing several modes (1:1, 1:2, 1:3, and 2:3) at ambient pressure (atm) and in vacuum. The substrate reference signal was recorded for an excitation 10 times stronger than for the membrane for best visibility.

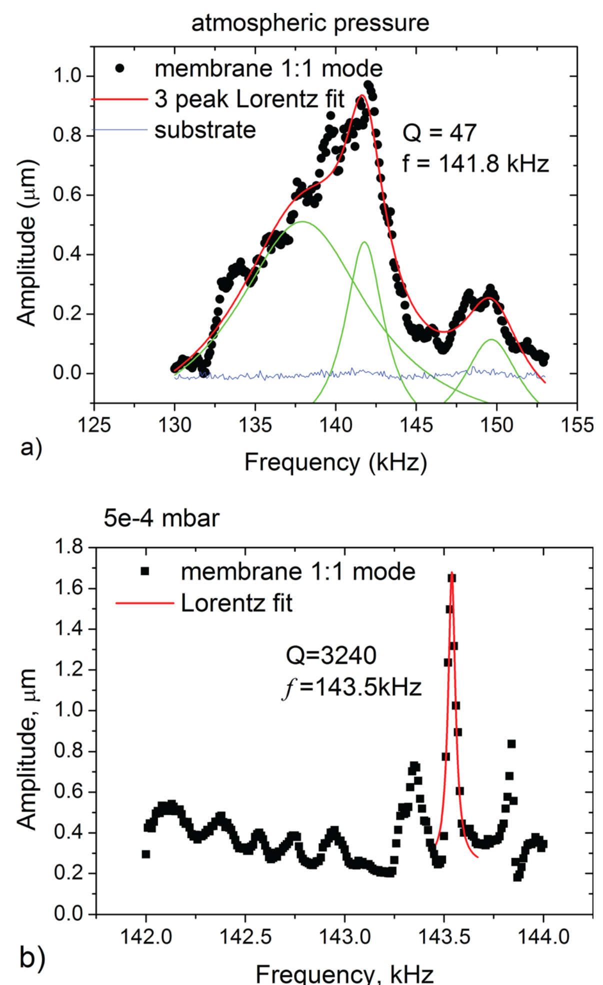


FIG. 10. The first vibrational mode of the studied membrane at (a) atmospheric and (b) $5 \times 10^{-4}$ millibars pressure, with Lorentzian peak fits. Multiple peaks are required to fit the mode at atmospheric pressure.

[This article is copyrighted as indicated in the article. Reuse of AIP content is subject to the terms at: http://scitation.aip.org/termsconditions. Downloaded to ] IP: 161.111.180.191 On: Tue, 15 Dec 2015 12:57:49

film and the substrate), the clamping losses (radiation losses into the substrate) are expected to be dominant. To give confidence in the Q factors determined, the strain throughout the membrane must be homogeneous; if not, the effect will influence damping and alter the measured results by skewing the modal distribution along the membrane.

## V. MEMBRANE STRAIN VARIATION

X-ray diffraction was used to determine the strain variation across the thick and ultra-thin membrane, using Bragg peaks from the Si substrate around the membrane as an absolute reference. Microdiffraction experiments were performed on beamline B16 at the DIAMOND Light Source, using X-rays with an energy of 12.4 keV ($\lambda = 1$ Å). A compound refractive lens was used to focus the X-ray beam with a footprint of 3 $\mu m^2$. The sample was mounted on a high precision *XYZ* stage in a five circle diffractometer, allowing the sample to be moved through the beam. Local heating caused by the beam has the potential to either damage the structures or distort the strain results by thermal expansion; therefore, to mitigate these effects the sample was actively cooled by a low-flow jet of nitrogen at 20 °C. Scattered X-rays were collected by a large PILATUS 300K detector. The 2D slice acquired by the PILATUS detector for a given angle of incidence ($\omega$) does not lie in the [001]–[110] plane in reciprocal space. RSMs as a function of position where obtained by rotating $\omega$ around the (004) reflection at each spatial point and rastering the sample through the beam. Both the ultra-thin and thick membranes were measured using (004) RSMs every 10 $\mu$m along the $[11\bar{0}]$ direction across the middle of the sample. Figure 11 shows the out-of-plane reciprocal space peak position. For comparison purposes, when Ge is pseudomorphically grown on Si, the misfit of the layer is −4.177% (where negative values represent compressive strain and positive values represent tensile). On the ultra-thin membrane edges, a sudden drop in $a_\perp$ of $1 \times 10^{-5}$ Å$^{-1}$ represents partial strain relaxation; the gradual decrease from 0.145% on the bulk to 0.142% on the membrane edge is within the experimental uncertainty of $5 \times 10^{-3}$%. Although the increase to 0.153% strain in the middle of the membrane is greater than this uncertainty, it is negligible in absolute terms. Although the increase in tensile strain is insufficient to significantly alter the bandstructure for electroluminescence, it is uniform across the entire platform. Furthermore, it can be seen that on the thick membrane, the difference in lattice parameter between edge and middle of the membrane is only $\sim 5 \times 10^{-6}$ Å$^{-1}$ which is within the experimental uncertainty and shows that the strain is almost completely homogeneous throughout the membrane, conforming that the measured Q-factor for the 800 nm membranes is highly reliable.

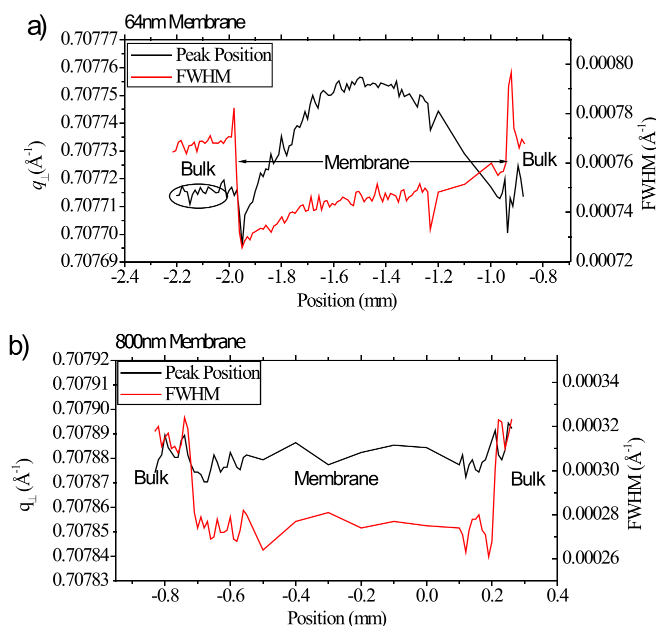


FIG. 11. The difference in peak position and the FWHM for the peak across both membranes: (a) 64 nm and (b) 800 nm.

Figure 11 also shows the FWHM of the diffraction peak for $q_\perp$ from both membranes. It has been shown that broadening of this peak is due to diffuse scattering from mosaicity[65] of the epilayer/substrate interface, where a variation of tilt exists due to the effective boundaries created by the misfit dislocation network. The edge effect on the profile for the ultra-thin membrane is less pronounced at the right hand side, because the sample was not mounted exactly flat on the sample stage but was slightly raised on the right-edge compared to the left-edge (seen as the slight drift in the FWHM). This result confirms that apart from at its edges, the membrane itself is free from tilt and is flat relative to the original Si wafer. This tilting effect is not present in the thicker membrane. We can see in both cases that the FWHM is 3–4 $\times 10^{-4}$ Å$^{-1}$ less for peaks from the freely suspended part of the membrane than from the supported part. We interpret this as showing that by removing the Ge/Si(001) interface, scattering from the misfit network has been eliminated. The overall relaxation during growth from pseudomorphic to tensile strained Ge is the same in both layers, therefore the misfit dislocation density prior to membrane fabrication would also have been the same; the similar reduction of FWHM for both membranes supports this conclusion.

## VI. PLAN VIEW TEM AND AFM

Plan view TEM (PVTEM) was performed on the ultra-thin membrane, as the thickness allows it to be electron transparent, using a JEOL JEM-2000FX TEM operating at 200 keV. A typical dark field PV-TEM image of the membrane in the (220) reflection is displayed in Figure 12(a), where the membrane, frame edge, and frame can be seen to contain dislocations. The threading dislocation density (TDD) can be calculated as approx. $3 \times 10^9$ cm$^{-2}$ from the straight through condition. The TDD is identical for the frame and suspended Ge; however, the misfit dislocation network that is observed at the Si/Ge interface largely disappears when the Si substrate is removed, confirming our previous speculation[29] that the misfit network is removed on etching. Hence, the crystalline quality at the bottom interface of the Ge layer is improved and so is electrical isolation by eliminating surface to surface conduction through dislocations.

[This article is copyrighted as indicated in the article. Reuse of AIP content is subject to the terms at: http://scitation.aip.org/termsconditions. Downloaded to ] IP: 161.111.180.191 On: Tue, 15 Dec 2015 12:57:49

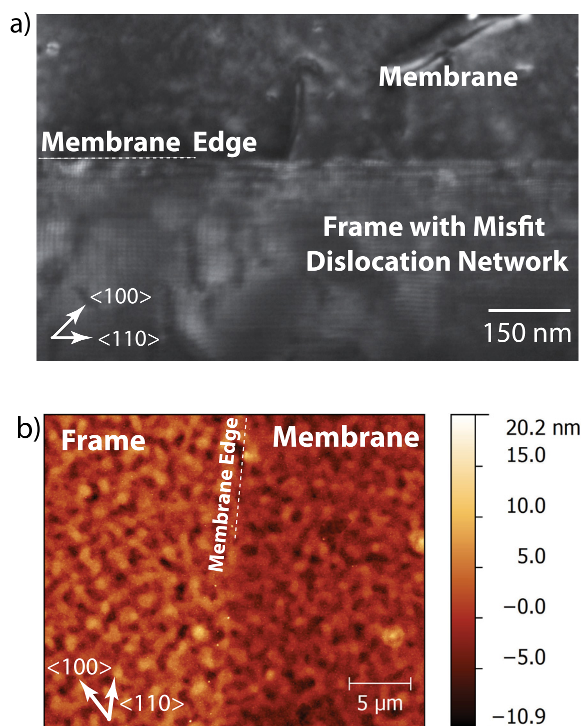


FIG. 12. (a) Dark field PVTEM of the 64 nm membrane at its edge in the (220) diffraction condition and (b) tapping mode AFM of the 64 nm membrane at its edge.

The surface morphology of the ultra-thin and thick membranes was measured using an Asylum Research MFP-3D-SA tapping mode AFM, with the morphology across the ultra-thin membrane and its frame edge shown in Figure 12(b). By taking a line profile across the ultra-thin membrane edge, a drop at the edge of approx. 2.5 nm is found. This recovers to the average height 45–50 $\mu$m away from the membrane edge; explaining the large tilt at the edge shown by the X-ray line profile. The measured RMS roughness of the frame is $2.66 \pm 0.05$ nm. However, the RMS roughness measured in the middle of the membrane has a lower value of $2.16 \pm 0.16$ nm. This suggests that the surface is actually modified due to the strain within the layer. This could also mean that the improvement in FWHM seen in the X-ray measurement was compounded by the smoother layer and removal of the misfit interface. However, we can eliminate this from measuring the roughness of the thicker membrane: The frame is measured to have an RMS roughness of $0.75 \pm 0.1$ nm, consistent with the as-grown layer, and the membrane itself has a roughness of $0.77 \pm 0.1$ nm. Since the two values agree within the experimental uncertainty, we speculate that the thicker membrane has enough overall rigidity to avoid surface modification. Hence, we conclude that the improvement in FWHM in the X-ray measurements (which was the same for both thicknesses) was mainly from removal of the misfit interface and not changing the surface roughness.

## VII. SUMMARY

In summary, a technique to fabricate ultra-thin (∼64 nm), crystalline, and flat Ge membrane has been demonstrated. In addition, we have presented evidence to show that the MEMS starting material strongly affects the limits which are placed on the fabrication process. When tensile strain is generated across the membrane, the final quality is extremely high and flat surfaces are obtained. The added advantage of epitaxial growth is that it provides control of the Ge membrane thickness and could be used as a platform for growing other heterostructures. We also show a bulk wafer process to fabricate ultra-thin ∼64 nm and thin∼250 nm membranes with relatively high yields of ∼50% across a 4 in. wafer. In addition, crystalline Ge is used as an etch mask which has a full coverage (without risk of pinholes) and can be grown at the lower temperature of 400 °C compared to 700 °C needed for high quality $SiO_2$ to be grown.

We report on the optical transmittance, reflectivity, and absorbance of thin and thick membranes from 450 nm to 1000 nm. Interference effects similar to a Fabry-Pérot optical cavity are particularly strong in the thinner membrane and that the transmittance threshold moves from 675 nm to 600 nm by reducing the thickness of the membrane Q factors of the thicker Ge membrane were studied using actuation by a piezoelectric transducer, with membrane displacement detection using a laser interferometer. Q factors of approximately 50 at atmospheric pressure and 3240 in vacuum were observed. The stress in the membrane was estimated to be 0.220 GPa from the frequencies of the observed vibrational modes, slightly larger than the value calculated from the lattice mismatch of 0.182 GPa. The vibration techniques confirmed that the stress was isotropic across the membranes, which is an important consideration when using these membranes for subsequent device growth or as MEMS platforms.

The crystalline quality of the membranes could also be assessed using the FWHM of the X-ray diffraction peak. It was found that simply by suspending the epitaxial Ge the crystalline quality was improved. By further microscopy techniques, it was ascertained that the misfit dislocation region was removed in the suspended membrane and that the surface of the ultra-thin membrane was smoother than the frame whereas the thicker membrane had no surface modification. The thick membrane was found to have many desirable qualities such as strain homogeneity, sub-nm roughness, and a low Q-factor to promote stability during agitation. These qualities suggest that such high quality Ge membranes could be ideal growth platforms as well as integration platforms. The principle of our method can also be applied to other materials and to smaller dimension systems for low cost MEMS fabrication.

## ACKNOWLEDGEMENTS

This work was carried out under the RCUK Basic Technology Programme supported by research Grant Nos. EP/F040784/1, EP/J001074/1, and EP/L007010/1. It also received funding from the European Community's Seventh Framework Programme (FP7/2007-2013) under Grant Agreement NANOFUNCTION n°257375 alongside funding from TAPHOR (MAT2012–31392) and FP7 Project MERGING (Grant No. 309150). Vibrational property

[This article is copyrighted as indicated in the article. Reuse of AIP content is subject to the terms at: http://scitation.aip.org/termsconditions. Downloaded to ] IP: 161.111.180.191 On: Tue, 15 Dec 2015 12:57:49

measurements were funded by the ERC under Grant No. 202735, NonContactUltrasonic. This research used equipment funded by AWM and ERDF through the Science City Energy Efficiency Project.


[1]K. Eshraghian, Proc. IEEE **94**(6), 1197–1213 (2006).
[2]S. J. Utteridge, V. A. Sashin, S. A. Canney, M. J. Ford, Z. Fang, D. R. Oliver, M. Vos, and E. Weigold, Appl. Surf. Sci. **162–163**, 359–367 (2000).
[3]T. Tritt, *Thermal Conductivity: Theory, Properties and Applications* (Springer, Clemson, South Carolina, 2004).
[4]B. Bhushan, *Handbook of Nanotechnology* (Springer, 2007).
[5]W. O. Davis, R. Sprague, and J. Miller, "MEMS-based pico projector display," in *IEEE/LEOS International Conference on Optical MEMs and Nanophotonics* (IEEE, New York, 2008).
[6]G. Rempe, R. J. Thompson, H. J. Kimble, and R. Lalezari, Opt. Lett. **17**(5), 363–365 (1992).
[7]J. M. Bustillo, R. T. Howe, and R. S. Muller, Proc. IEEE **86**(8), 1552–1574 (1998).
[8]R. M. Sieg, J. A. Carlin, J. J. Boeckl, S. A. Ringel, M. T. Currie, S. M. Ting, T. A. Langdo, G. Taraschi, E. A. Fitzgerald, and B. M. Keyes, Appl. Phys. Lett. **73**(21), 3111–3113 (1998).
[9]J. M. Hartmann, A. Abbadie, A. M. Papon, P. Holliger, G. Rolland, T. Billon, J. M. Fedeli, M. Rouviere, L. Vivien, and S. Laval, J. Appl. Phys. **95**(10), 5905–5913 (2004).
[10]J. Liu, R. Camacho-Aguilera, J. T. Bessette, X. Sun, X. Wang, Y. Cai, L. C. Kimerling, and J. Michel, Thin Solid Films **520**(8), 3354–3360 (2012).
[11]J. F. Liu, X. C. Sun, R. Camacho-Aguilera, L. C. Kimerling, and J. Michel, Opt. Lett. **35**(5), 679–681 (2010).
[12]R. R. King, D. C. Law, K. M. Edmondson, C. M. Fetzer, G. S. Kinsey, H. Yoon, R. A. Sherif, and N. H. Karam, Appl. Phys. Lett. **90**(18), 183516 (2007).
[13]D. Nam, D. Sukhdeo, A. Roy, K. Balram, S. L. Cheng, K. C. Y. Huang, Z. Yuan, M. Brongersma, Y. Nishi, D. Miller, and K. C. Saraswat, Opt. Express **19**(27), 25866–25872 (2011).
[14]N. Amrane, S. A. Abderrahmane, and H. Aourag, Infrared Phys. Technol. **36**(5), 843–848 (1995).
[15]R. M. Audet, E. H. Edwards, K. C. Balram, S. A. Claussen, R. K. Schaevitz, E. Tasyurek, R. Yiwen, E. I. Fei, T. I. Kamins, J. S. Harris, and D. A. B. Miller, J. Lightwave Technol. **31**(24), 3995–4003 (2013).
[16]C. Boztug, J. R. Sánchez-Pérez, F. F. Sudradjat, R. B. Jacobson, D. M. Paskiewicz, M. G. Lagally, and R. Paiella, Small **9**(4), 622–630 (2013).
[17]F. Cavallo and M. G. Lagally, Nanoscale Res. Lett. **7**, 1–10 (2012).
[18]J. R. Sánchez-Pérez, C. Boztug, F. Chen, F. F. Sudradjat, D. M. Paskiewicz, R. Jacobson, M. G. Lagally, and R. Paiella, Proc. Natl. Acad. Sci. U. S. A. **108**(47), 18893–18898 (2011).
[19]M. Huang, F. Cavallo, F. Liu, and M. G. Lagally, Nanoscale **3**(1), 96–120 (2011).
[20]E. Thielicke and E. Obermeier, Mechatronics **10**(4–5), 431–455 (2000).
[21]A. I. Fedorchenko, A. B. Wang, V. I. Mashanov, and H. H. Cheng, J. Mech. **21**(3), 131–135 (2005).
[22]K. C. Lee, J. Electrochem. Soc. **137**(8), 2556–2574 (1990).
[23]M. Myronov, A. Dobbie, V. A. Shah, X. C. Liu, V. H. Nguyen, and D. R. Leadley, Electrochem. Solid-State Lett. **13**(11), H388–H390 (2010).
[24]V. A. Shah, A. Dobbie, M. Myronov, D. J. F. Fulgoni, L. J. Nash, and D. R. Leadley, Appl. Phys. Lett. **93**(19), 192103 (2008).
[25]V. A. Shah, M. Myronov, A. Dobbie, and D. R. Leadley, ECS J. Solid State Sci. Technol. **2**(3), Q40–Q44 (2013).
[26]Y. A. Osip'yan and S. A. Shevchenko, JETP Lett. **20**(11), 328–329 (1974), available at http://www.jetpletters.ac.ru/ps/1794/article_27391.shtml.
[27]J. Hess, J. Schreiber, S. Hildebrandt, and R. Labusch, Phys. Status Solidi B **172**(1), 225–234 (1992).
[28]S. A. Shevchenko, J. Exp. Theor. Phys. **88**(1), 66–71 (1999).
[29]V. A. Shah, M. Myronov, C. Wongwanitwatana, L. Bawden, M. J. Prest, J. S. Richardson-Bullock, S. Rhead, E. H. C. Parker, T. E. Whall, and D. R. Leadley, Sci. Technol. Adv. Mater. **13**(5), 055002 (2012).
[30]T. A. Langdo, M. T. Currie, Z. Y. Cheng, J. G. Fiorenza, M. Erdtmann, G. Braithwaite, C. W. Leitz, C. J. Vineis, J. A. Carlin, A. Lochtefeld, M. T. Bulsara, I. Lauer, D. A. Antoniadis, and M. Somerville, Solid-State Electron. **48**(8), 1357–1367 (2004).
[31]A. Shchepetov, M. Prunnila, F. Alzina, L. Schneider, J. Cuffe, H. Jiang, E. I. Kauppinen, C. M. S. Torres, and J. Ahopelto, Appl. Phys. Lett. **102**(19), 192108 (2013).
[32]S. D. Collins, J. Electrochem. Soc. **144**(6), 2242–2262 (1997).
[33]M. Elwenspoek and H. Jansen, *Silicon Micromachining* (Cambridge University Press, Cambridge, 1998).
[34]B. Li, B. Xiong, L. N. Jiang, Y. Zohar, and M. Wong, J. Microelectromech. Syst. **8**(4), 366–372 (1999).
[35]M. Sasaki, T. Sasaki, H. Kazuhiro, and M. Hideo, J. Opt. A: Pure Appl. Opt. **10**(4), 044004 (2008).
[36]V. A. Shah, A. Dobbie, M. Myronov, and D. R. Leadley, Solid-State Electron. **62**(1), 189–194 (2011).
[37]V. A. Shah, A. Dobbie, M. Myronov, and D. R. Leadley, J. Appl. Phys. **107**(6), 064304 (2010).
[38]B. Hollander, D. Buca, S. Mantl, and J. M. Hartmann, J. Electrochem. Soc. **157**(6), H643–H646 (2010).
[39]O. Tabata, R. Asahi, H. Funabashi, K. Shimaoka, and S. Sugiyama, Sens. Actuators, A **34**(1), 51–57 (1992).
[40]F. Laermer, A. Schilp, K. Funk, and M. Offenberg, in *Proceedings of the IEEE Micro-Electronics* (IEEE, New York, 1999), pp. 211–216.
[41]H. R. Philipp and E. A. Taft, Phys. Rev. **113**(4), 1002–1005 (1959).
[42]S. S. Verbridge, H. G. Craighead, and J. M. Parpia, Appl. Phys. Lett. **92**(1), 013112 (2008).
[43]S. S. Verbridge, J. M. Parpia, R. B. Reichenbach, L. M. Bellan, and H. G. Craighead, J. Appl. Phys. **99**(12), 124304 (2006).
[44]S. S. Verbridge, D. F. Shapiro, H. G. Craighead, and J. M. Parpia, Nano Lett. **7**(6), 1728–1735 (2007).
[45]D. J. Wilson, C. A. Regal, S. B. Papp, and H. J. Kimble, Phys. Rev. Lett. **103**(20), 207204 (2009).
[46]I. Wilson-Rae, R. A. Barton, S. S. Verbridge, D. R. Southworth, B. Ilic, H. G. Craighead, and J. M. Parpia, Phys. Rev. Lett. **106**(4), 047205 (2011).
[47]V. Sazonova, Y. Yaish, H. Ustunel, D. Roundy, T. A. Arias, and P. L. McEuen, Nature **431**(7006), 284 (2004).
[48]P. Poncharal, Z. L. Wang, D. Ugarte, and W. A. de Heer, Science **283**(5407), 1513–1516 (1999).
[49]B. Reulet, A. Y. Kasumov, M. Kociak, R. Deblock, I. I. Khodos, Y. B. Gorbatov, V. T. Volkov, C. Journet, and H. Bouchiat, Phys. Rev. Lett. **85**(13), 2829–2832 (2000).
[50]R. Gao, Z. L. Wang, Z. Bai, W. A. de Heer, L. Dai, and M. Gao, Phys. Rev. Lett. **85**(3), 622–625 (2000).
[51]S. T. Purcell, P. Vincent, C. Journet, and V. T. Binh, Phys. Rev. Lett. **89**(27), 276103 (2002).
[52]V. Singh, S. Sengupta, H. S. Solanki, R. Dhall, A. Allain, S. Dhara, P. Pant, and M. M. Deshmukh, Nanotechnology **21**(16), 165204 (2010).
[53]J. S. Bunch, A. M. van der Zande, S. S. Verbridge, I. W. Frank, D. M. Tanenbaum, J. M. Parpia, H. G. Craighead, and P. L. McEuen, Science **315**(5811), 490–493 (2007).
[54]J. S. Bunch, S. S. Verbridge, J. S. Alden, A. M. van der Zande, J. M. Parpia, H. G. Craighead, and P. L. McEuen, Nano Lett. **8**(8), 2458 (2008).
[55]R. A. Barton, B. Ilic, A. M. van der Zande, W. S. Whitney, P. L. McEuen, J. M. Parpia, and H. G. Craighead, Nano Lett. **11**(3), 1232–1236 (2011).
[56]S. Shivaraman, R. A. Barton, X. Yu, J. Alden, L. Herman, M. V. S. Chandrashekhar, J. Park, P. L. McEuen, J. M. Parpia, H. G. Craighead, and M. G. Spencer, Nano Lett. **9**(9), 3100 (2009).
[57]J. T. Robinson, M. Zalalutdinov, J. W. Baldwin, E. S. Snow, Z. Q. Wei, P. Sheehan, and B. H. Houston, Nano Lett. **8**(10), 3441 (2008).
[58]A. Eichler, J. Moser, J. Chaste, M. Zdrojek, I. W. Rae, and A. Bachtold, Nat. Nanotechnol. **6**(6), 339–342 (2011).
[59]X. Liu, J. F. Vignola, H. J. Simpson, B. R. Lemon, B. H. Houston, and D. M. Photiadis, J. Appl. Phys. **97**(2), 023524 (2005).
[60]T. Mattila, J. Kiihamäki, T. Lamminmäki, O. Jaakkola, P. Rantakari, A. Oja, H. Seppä, H. Kattelus, and I. Tittonen, Sens. Actuators, A **101**(1–2), 1–9 (2002).
[61]A. E. Franke, J. M. Heck, K. Tsu-Jae, and R. T. Howe, J. Microelectromech. Syst. **12**(2), 160–171 (2003).
[62]R. B. Bhiladvala and Z. J. Wang, Phys. Rev. E **69**(3), 036307 (2004).
[63]M. Karnezos, J. Vac. Sci. Technol., B: Microelectron. Nanometer Struct. **4**(1), 226–229 (1986).
[64]E. Forsen, G. Abadal, S. Ghatnekar-Nilsson, J. Teva, J. Verd, R. Sandberg, W. Svendsen, F. Perez-Murano, J. Esteve, E. Figueras, F. Campabadal, L. Montelius, N. Barniol, and A. Boisen, Appl. Phys. Lett. **87**(4), 043507 (2005).
[65]S. Mochizuki, A. Sakai, N. Taoka, O. Nakatsuka, S. Takeda, S. Kimura, M. Ogawa, and S. Zaima, Thin Solid Films **508**(1–2), 128–131 (2006).


[This article is copyrighted as indicated in the article. Reuse of AIP content is subject to the terms at: http://scitation.aip.org/termsconditions. Downloaded to ] IP: 161.111.180.191 On: Tue, 15 Dec 2015 12:57:49